

# A softer look at MCG–6-30-15 with *XMM-Newton*

A. K. Turner<sup>1\*</sup>, A. C. Fabian<sup>1</sup>, S. Vaughan<sup>1</sup> and J. C. Lee<sup>2</sup>

<sup>1</sup>Institute of Astronomy, Madingley Road, Cambridge CB3 0HA

<sup>2</sup>Chandra Fellow, Massachusetts Institute of Technology, Center for Space Research, 77 Massachusetts Ave. NE80, Cambridge, MA 02139, USA

27 October 2018

## ABSTRACT

We present the analysis and first results from the Reflection Grating Spectrometer (RGS) during the 320 ks *XMM-Newton* observation of the Seyfert 1 galaxy MCG–6-30-15. The spectrum is marked by a sharp drop in flux at 0.7 keV which has been interpreted by Branduardi-Raymont et al. using RGS spectra from an earlier and shorter observation as the blue wing of a strong relativistic OVIII emission line and by Lee et al. using a *Chandra* spectrum as due to a dusty warm absorber. We find that the drop is well explained by the FeI  $L_{2,3}$  absorption edges and obtain reasonable fits over the 0.32–1.7 keV band using a multi-zone, dusty warm absorber model constructed using the photoionization code CLOUDY. Some residuals remain which could be due to emission from a relativistic disc, but at a much weaker level than from any simple model relying on relativistic emission lines alone. A model based on such emission lines can be made to fit if sufficient (warm) absorption is added, although the line strengths exceed those expected. In order to distinguish further whether the spectral shape is dominated by absorption or emission, we examined the difference spectrum between the highest and lowest flux states of the source. The EPIC pn data indicate that this is a power-law in the 3–10 keV band which, if extrapolated to lower energies, reveals the absorption function acting on the intrinsic spectrum, provided that any emission lines do not scale exactly with the continuum. We find that this function matches our dusty warm absorber model well if the power-law steepens below 2 keV. The soft X-ray spectrum is therefore dominated by absorption structures, with the equivalent width of any individual emission lines in the residuals being below about 30 eV.

**Key words:** galaxies: active – galaxies: Seyfert: general – galaxies: individual: MCG–6-30-15 – X-ray: galaxies

## 1 INTRODUCTION

MCG–6-30-15 is one of the most studied Seyfert 1 galaxies in the X-ray band due to its high X-ray flux and relative closeness ( $z = 0.00775$ ,  $L_{2-10 \text{ keV}} \sim 5 \times 10^{42} \text{ erg s}^{-1}$ ;  $H_0 = 70 \text{ km s}^{-1} \text{ Mpc}^{-1}$ ). At energies above 2 keV the X-ray spectrum consists of a power-law with  $\Gamma \simeq 1.9$ , skewed iron  $K\alpha$  line and reflection hump (e.g. Fabian et al. 2002). At softer energies much controversy still exist concerning the observed spectral features. Before the use of grating spectra, sharp drops in flux observed in soft X-ray spectra were interpreted as absorption edges due to OVII and OVIII in ionized gas within the AGN environment (“the warm absorber”; Otani et al. 1996; Reynolds 1997; George et al. 1998).

However the increase in spectral resolution afforded by the use of grating spectrometers onboard *XMM-Newton* and *Chandra* has challenged the view that reprocessing of soft X-rays by photoionized gas is responsible for the observed spectral features. Branduardi-Raymont et al. (2001) proposed that sharp drops seen

in the Reflection Grating Spectrometer (RGS) spectra from *XMM-Newton* observations of MCG–6-30-15 and Mrk 766 at  $\sim 0.39$ ,  $\sim 0.55$  and  $\sim 0.7$  keV were due to the blue wings of relativistically blurred emission lines of CVI, NVII and OVIII  $\text{Ly}\alpha$ , the blurring mechanism being the same as that used to explain the skewness of the Fe  $K\alpha$  line. The reason for adopting this view was that the position of the sharp drop at  $\sim 0.7$  keV, if caused by an OVII absorption edge inferred an unrealistically high infall velocity of matter of  $\sim 16,000 \text{ km s}^{-1}$ . Lee et al. (2001) countered this suggestion with *Chandra* High Energy Transmission Grating Spectrometer (HETGS) observations in which the  $16,000 \text{ km s}^{-1}$  discrepancy in position of the OVII edge was explained by the blending together of resonance absorption lines red-ward of the edge and by L-shell absorption from neutral iron which is probably in the form of dust (the “dusty warm absorber” model; DWA). In a re-analysis of the original RGS data Sako et al. (2003) fitted both the DWA and blurred emission line models to the original RGS data. These workers argue that the models of Lee et al. (2001) over-predicted the flux below the passband of the HETG instrument and that the relativistic line

\* E-mail: akt21@ast.cam.ac.uk

interpretation provides a better fit to the data than the DWA interpretation.

Given the evidence for a relativistically-blurred iron line and reflection continuum in MCG–6–30–15, some relativistically-blurred soft X-ray lines are also expected in the spectrum (Ross & Fabian 1993; Nayakshin, Kazanas, & Kallman 2000; Rózańska et al. 2002). The strength of these lines is however predicted to be much smaller, and the blue wing broader, than those claimed from the RGS spectra (Ballantyne, Ross, & Fabian 2002). The determination of the underlying soft X-ray continuum is of importance for understanding the X-ray irradiation of accretion discs.

This paper presents the RGS data for the long  $\sim 320$  ks observation of MCG–6–30–15 (Fabian et al. 2002). In particular we test to see if a DWA or relativistically-blurred emission line model can explain the overall spectral shape and see what can be inferred about the underlying continuum. The rest of the paper is organised as follows. Section 2 describes the data reduction. In Section 3 absorption across the 0.7 keV drop is examined. Section 4 presents a photoionization model of the warm absorber used in Section 5, where DWA and the relativistically-blurred emission line models are fit to the data. In Section 6 an attempt is made to use spectral variability to determine the underlying continuum. The results are discussed in Section 7. This paper does not represent a full description of the data but a first step in modelling the RGS spectrum of the DWA in MCG–6–30–15 and a first look at some of the key features in the data. Plasma diagnostics of individual species will be presented in a later paper.

## 2 DATA REDUCTION

MCG–6–30–15 was observed by *XMM-Newton* on revolutions 301, 302 and 303 (2001 July 31 – 2001 August 5) for 320 ks (Fabian et al. 2002). The observation data files (ODFs) were reduced with version 5.3.3 of the *XMM-Newton* Science Analysis Software (SAS) using the standard processing chains and the calibrations from 2002 December. The final few ks of data from each revolution showed strong background flaring, these periods were removed from the data extraction. The data were grouped so that at least 20 counts were in each bin and were fitted to trial models in XSPEC v11.2 (Arnaud 1996). Data above 1.7 keV were ignored due to the known calibration uncertainties at the mirror Au edge. Unless otherwise stated errors quoted are for 90 per cent confidence level for one interesting parameter ( $\Delta\chi^2 = 2.7$ ). The data are plotted in the observation frame throughout.

## 3 SIMPLE ABSORPTION MODEL

The fluxed RGS spectrum from all three revolutions is shown in Fig. 1. Evident in the spectra are the drops in flux at 0.39, 0.54 and 0.7 keV. The high spectral resolution of the RGS requires the inclusion of individual resonance absorption lines when considering the effect of photoionized absorption. Specifically, at the red side of an absorption edge there is a series of resonant absorption lines that converge to the edge energy. These have the effect of reducing the observed edge energy when convolved with intrinsic Doppler broadening and the spectral resolution of the instrument.

Models of the cross-section of OVII and OVIII near their K-edges were constructed using the continuum cross-section fitting formulae of Verner & Yakovlev (1995), the resonance absorption

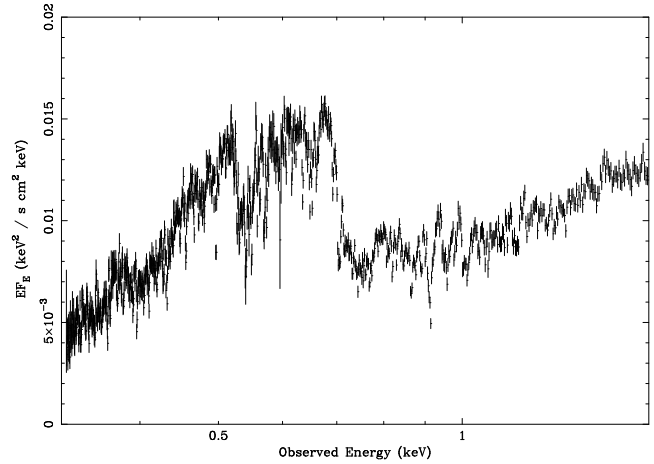


**Figure 1.** Combined and fluxed RGS data from all three satellite revolutions.

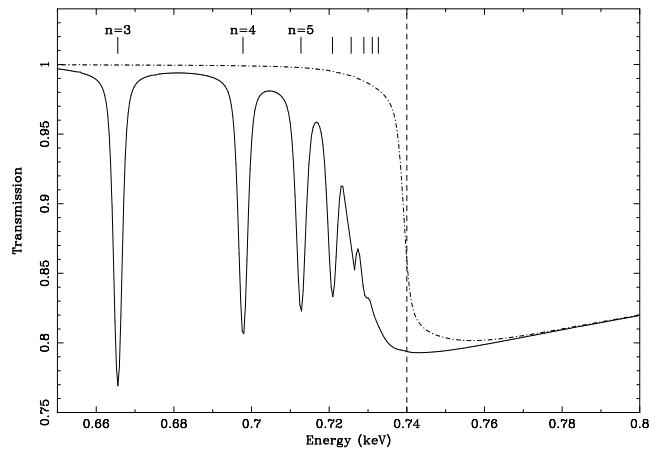


**Figure 2.** Detail of the predicted absorption near the OVII K-edge convolved with the RGS resolution for an OVII column density of  $10^{18} \text{ cm}^{-2}$  and turbulent velocity of  $100 \text{ km s}^{-1}$ . (solid): Absorption including photoelectric edge and  $1s^2 - 1snp$  resonance lines, (dot-dash): Absorption including photoelectric edge only, (dash): Position of OVII K-edge.

line data of Verner et al. (1996) and the fitting formulae for line absorption series near absorption edges of Mewe (1977). The transmission through a column density of  $10^{18} \text{ cm}^{-2}$  of OVII, calculated assuming a turbulent velocity (b parameter) of  $100 \text{ km s}^{-1}$ , is plotted in Fig. 2. This shows the effect of the resonance lines on the apparent position of the edge, which is clearly shifted to lower energies. Also present at 0.7 keV are the FeI L-shell absorption edges which have fine structure in their cross-section at the  $L_{2,3}$  edge as described by Kortricht & Kim (2000).

Fig. 3 shows the revolution 301 data fitted to a power-law, Galactic absorption ( $N_{\text{H}} = 4.06 \times 10^{20} \text{ cm}^{-2}$ ; Elvis, Wilkes, & Lockman 1989) and absorption by OVII, OVIII and FeI across the energy range 0.6 – 1.7 keV. The best fit ( $\chi^2 = 9003.9$  for 6625 degrees of freedom (*dof*)) requires a photon index of  $\Gamma = 2.36 \pm 0.02$  and column densities of  $\log N_{\text{OVII}} = 18.22 \pm 0.02$ ,  $\log N_{\text{OVIII}} = 18.47 \pm 0.02$  and  $\log N_{\text{FeI}} = 17.29 \pm 0.02$ . Although the best fitting model gives a poor overall  $\chi^2_{\nu}$ , it reproduces the detailed shape of the drop at  $\sim 0.7$  keV remarkably well as can be seen from Fig. 4 where the model is compared to the fluxed spectrum from all three orbits. The sharp drops at 0.7 and

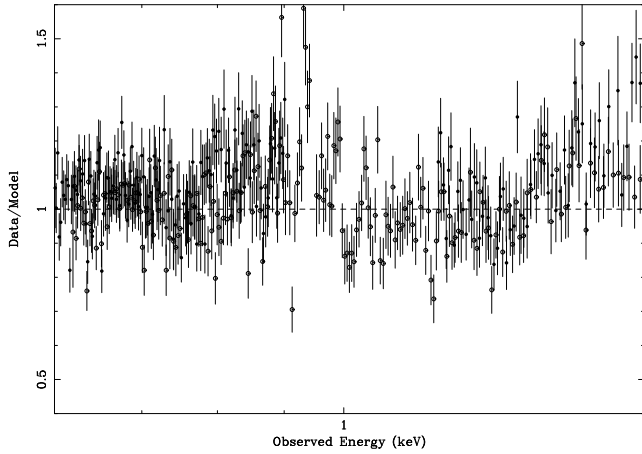


**Figure 3.** Ratio of data for (filled circles) RGS1 and (open circles) RGS2 from orbit 301 to a model consisting of a power-law, Galactic absorption and OVII, OVIII and FeI absorption.

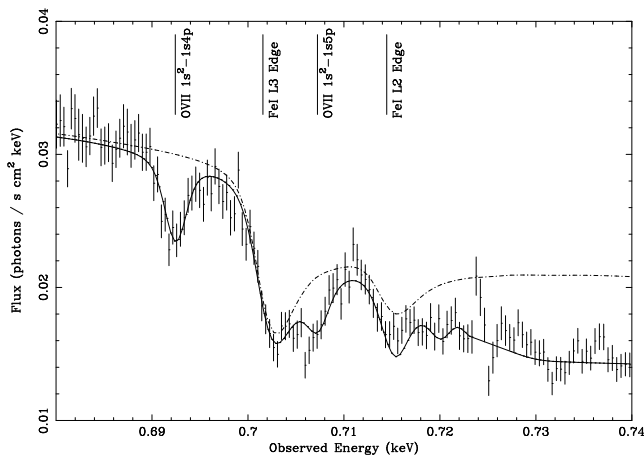


**Figure 4.** Details of fluxed spectrum for all three orbits compared to a model of OVII, OVIII and FeI absorption (solid) and FeI absorption only (dash-dot).

0.713 keV are clearly fitted by the Fe I absorption profile. Also evident are the resonant absorption lines of OVII. The Fe I  $L_3$  edge is observed at  $0.7023 \pm 0.0007$  keV which corresponds to a velocity of  $-320 \pm 340$  km s $^{-1}$  with respect to the rest frame of the source if the iron is in the metallic form described by Kortricht & Kim (2000). The absolute error on the energy scale of measurements of the cross-section of iron oxides are required before it can be determined whether the observed iron is in the metallic or iron oxide form. The derived power-law photon index is higher than the photon index of  $\sim 1.9$  derived with the EPIC instrument above 2.5 keV (Fabian et al. 2002) suggesting the emission below 1–2 keV has a soft excess relative to an extrapolation of the best fitting continuum above 2 keV (see also Lee et al. 2001). The residuals around 1 keV are due to absorption lines of FeXIII–XXIV and NeIX–X.

#### 4 PHOTOIONIZATION MODEL

While the previous Section suggests that absorption by FeI, OVII and OVIII can explain the sharp drop in flux at 0.7 keV, it does not provide a self-consistent model of absorption from a photoionized

absorber. In order to explore the properties of any warm absorption in MCG–6–30–15 and provide a model of this absorption the 96beta5 version of the photoionization code CLOUDY was used to calculate the absorbed spectrum produced by the passage of a continuum through a layer of gas (Ferland et al. 1998). This version of CLOUDY was used since it includes the atomic transitions of the iron Unresolved Transition Array (UTA; Behar, Sako, & Kahn 2001) which have been observed previously in Seyfert 1 X-ray spectra. Above 1 keV the incident continuum is taken to have the spectral shape inferred from fitting the EPIC and *BeppoSAX* data (Fabian et al. 2002). Below 1.0 keV the spectrum is assumed to be a power-law with  $\Gamma = 2.0–3.0$  down to a break energy of 10 eV and  $\Gamma = -1.5$  below this. The normalization of the incident spectrum is determined from the X-ray luminosity in the 2–10 keV range,  $L_{2-10}$ , inferred from the EPIC and *BeppoSAX* data. Also included in the incident continuum is a blackbody component with a temperature of  $2.5 \times 10^5$  K and bolometric luminosity of  $6 \times 10^{43}$  erg s $^{-1}$ . The gas is assumed to have a constant density and Solar elemental abundance with a turbulent velocity of 100 km s $^{-1}$ . This turbulent velocity is used since the lines appear unresolved in the *Chandra* HETGS spectrum of Lee et al. (2001).

The code was used to generate a grid of incident and absorbed spectra as well as a list of absorption line optical depths at line centre where greater than 0.01. The parameters that were varied across the grid were column density of the gas ( $N_H = 10^{20} - 10^{22}$  cm $^{-2}$ ), inner radius of cloud from central source ( $R = 10^{16} - 10^{19}$  cm), ionization parameter of the cloud ( $\xi = 10^{-5} - 10^3$ ) and spectral index between 10 eV and 1 keV ( $\Gamma = 2.0 - 3.0$ ). The density of the gas,  $n_H$ , is set from  $R$ ,  $\xi$  and  $L_{2-10}$ , through the formula:

$$\xi = \frac{L_{2-10}}{n_H R^2}$$

The resulting transmitted continua (i.e. including only bound-free edges) were divided by the incident continua to produce a continuum absorption model. The absorption lines were then included using a Gaussian opacity profile with a b width of 100 km s $^{-1}$ .

In using only the turbulent velocity as the line broadening mechanism the natural and thermal broadening of the lines are neglected. Thermal broadening is ignored since for the species of interest in a photoionized gas thermal broadening velocities are only 10–20 per cent of the turbulent velocity (Nicastro, Fiore, & Matt 1999). Lee et al. (2001) show that various absorption lines from OVII and OVIII lie on the flat part of the curve of growth for column densities of interest here, justifying our neglect of natural line broadening.

## 5 SPECTRAL FITTING

### 5.1 Dusty warm absorber model

We now fit the warm absorber photoionization model to the data from all three revolutions. Galactic absorption, FeI absorption and multiple warm absorption zones are included to account for absorption of the continuum. The absorption component is kept fixed between data from different revolutions while the parameters of the underlying continuum are allowed to vary. The continuum is taken to be a broken power-law with a break energy of 1 keV, spectral index of 2.2 above the break energy and a variable spectral index below the break energy. The use of a broken power-law is justified since the variability suggests some break in the continuum at

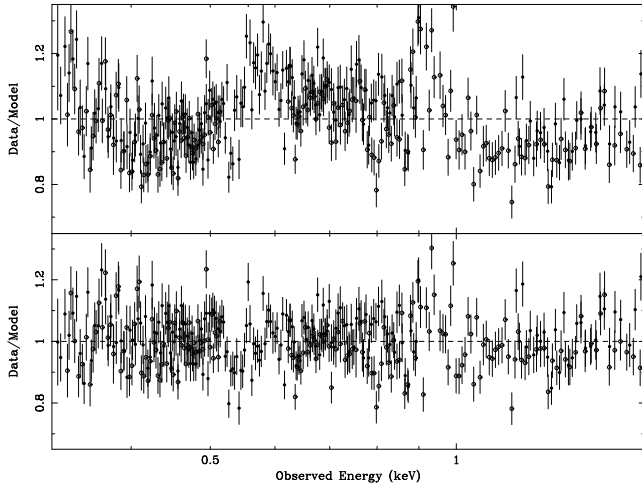


**Figure 5.** Ratio of data from RGS1 (*filled circles*) and RGS2 (*open circles*) to the best fitting DWA models. Only data for orbit 301 is shown here. (a) Four zone DWA model with underlying broken power-law. (b) Four zone DWA model with underlying broken power-law and excess broad emission at  $\sim 0.56$  keV.

$\sim 1 - 2$  keV (Fabian et al. 2002; Fabian & Vaughan 2003). Fitting in the range 0.6–1.7 keV with a three zone warm absorber gives  $\chi^2 = 8412.6/6620$  *dof*. The fit parameters for this model are given in Table 1 (model 1). Three zones are required since two distinct velocity components are seen in the absorption lines (Sako et al. 2003) and features from a broad range of ionization parameters are present. Extending the model over the whole RGS passband reveals that the predicted model flux is far higher than the observed data below 0.5 keV. The smooth nature of the discrepancy suggests additional cold absorption is needed, possibly in the form of absorption from the ISM within MCG–6–30–15. However, including additional cold absorption in our fit to the 0.32–1.7 keV energy range produces a large OI edge that is not seen in the data. One possibility is that gas is partly ionized so most of the O is ionized to higher species reducing the depth of the OI edge. A four zone warm absorber produces a fit with  $\chi^2 = 16601.9/12053$  *dof*, where one of the zones has a low ionization parameter  $\log \xi = -4.4$  accounting for the excess low energy absorption. Table 1 (model 2) gives the fit parameters for this model. The residuals for this model are shown in Fig. 5a. As mentioned the lowest ionization parameter zone is required to cause the spectrum to turn down at low energies without too deep a neutral oxygen edge. The medium ionization parameter zone is required to fit the OVII edge and lines, the drop in flux at  $\sim 0.39$  keV due to the CV edge and the Fe UTA at 0.7–0.8 keV which takes the form of a trough in the data. The higher parameter zones are required to fit a range of absorption line features around 1 keV as well as any OVIII features. The majority of the OVII column density is located in zone 2 ( $\log \xi \sim -0.5$ ) while the majority of the OVIII column density is located in the highest ionization parameter zones 3 and 4 ( $\log \xi \sim 1.5$ ). The best fitting DWA model contains less OVII and OVIII column density than the simple absorption model presented in section 3 since other absorption components are present in the photoionization models, such as the Fe UTA, that can compensate for some of the OVII and OVIII column. Although residuals are present they take the form of broad features, whereas the region across the 0.7 keV drop is reasonably well fitted.

We now add a broad Gaussian emission component at  $\sim 0.6$  keV to account for any excess emission in this region possi-

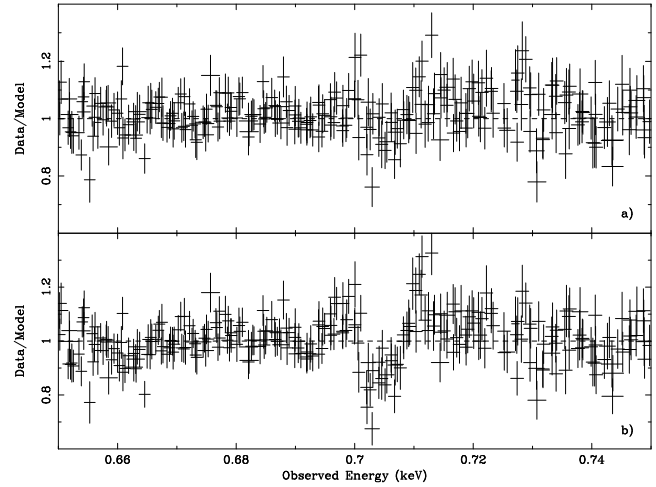


**Figure 6.** (a) Detail of residuals for the best fitting DWA model in the 0.65–0.75 keV region. The six data sets are shown simultaneously (one from each revolution and instrument). (b) Same as (a) except for the best fitting REL model.

bly from reflection components. The best-fitting model produces a significant improvement in the fit with  $\chi^2 = 15977.3/12051$  *dof* as can be seen in Fig. 5b (see model 3 in Table 1 for the fit parameters of this model). The line has an equivalent width of  $\sim 120$  eV and is very broad with  $\sigma \sim 170$  eV. The model fits the region around the 0.7 keV drop extremely well (see Fig. 6a). However, the broad Gaussian shape is not that of a single relativistic disc line and should be considered as only an approximation of the shape of the residuals. Adding the broad Gaussian emission line results in changes to the best fitting DWA component. The broad emission line has the effect of fitting the excess in the residuals in the range  $\sim 0.5$ –0.9 keV. This produces an excess below  $\sim 0.4$  keV and above  $\sim 1.35$  keV. The DWA component compensates to fit these excesses by, at low energy, increasing the ionisation parameter of the lowest ionization parameter zone (zone 1) which results in absorption that rolls over less at low energies and is flatter, and at high energies by decreasing the column density of the high ionization parameter zones which results in less absorption above  $\sim 1.35$  keV flattening the absorption.

## 5.2 Relativistic emission line model

Branduardi-Raymont et al. (2001) and Sako et al. (2003) argue that the drop in flux at 0.7 keV is due to the blue wing of a relativistically blurred OVIII Ly $\alpha$  emission line. In this interpretation the warm absorber is responsible for only narrow absorption features rather than any broad ionization edges. In this section we fit this relativistic emission line (REL) model to data from all three revolutions. In the original model of Branduardi-Raymont et al. (2001) the model consists of a power-law and emission lines due to CVI Ly $\alpha$  (0.368 keV), NVII Ly $\alpha$  (0.500 keV), and OVIII Ly $\alpha$  (0.654 keV) emitted by the inner-part of an accretion disc around a rotating black hole. The relativistic blurring is achieved with the LAOR model (Laor 1991). Free parameters in the model are inner and outer radius of the disc ( $R_{\text{in}}$  and  $R_{\text{out}}$ ), disc inclination ( $i$ ), emissivity  $\epsilon$  as a function of radius  $R$  which is parametrized as a power-law with index  $q$  (i.e.  $\epsilon \propto R^{-q}$ ). Galactic absorption is also included. The best fitting model produces a fit with  $\chi^2 = 17457.8/12051$  *dof* (see Fig. 7a). The fit parameters of this model are given in Table 2 (model 1). While the level of the continuum is

**Table 1.** Results of fits of the DWA model to all three revolutions of RGS data. Line energy of the broad Gaussian emission line ( $E_g$ ) is given in units of keV. Width ( $\sigma_g$ ) and equivalent width ( $EW_g$ ) of the broad Gaussian emission line are given in eV. Column density ( $N_X$ ) is given in units of  $\log \text{cm}^{-2}$ . Velocity ( $v$ ) is given in  $\text{km s}^{-1}$ .

model	zone	1	2	3
$\Gamma_1$		$2.72 \pm 0.03$	$2.91 \pm 0.02$	$2.68 \pm 0.04$
$E_g$		–	–	$0.54 \pm 0.03$
$\sigma_g$		–	–	$176 \pm 15$
$EW_g$		–	–	$121 \pm 12$
$N_{\text{FeI}}$		$17.28 \pm 0.03$	$17.22 \pm 0.02$	$17.25 \pm 0.03$
$N_{\text{H}}$	1	$21.37 \pm 0.04$	$20.86 \pm 0.01$	$21.12 \pm 0.04$
$\log \xi$	1	$-0.47 \pm 0.03$	$-4.42 \pm 0.23$	$-1.92 \pm 0.02$
$v$	1	$0^f$	$0^f$	$0^f$
$N_{\text{H}}$	2	$21.72 \pm 0.05$	$21.44 \pm 0.03$	$21.44 \pm 0.03$
$\log \xi$	2	$1.43 \pm 0.03$	$-0.52 \pm 0.02$	$-0.36 \pm 0.03$
$v$	2	$0^f$	$0^f$	$0^f$
$N_{\text{H}}$	3	$22.00^f$	$22.00^f$	$21.73 \pm 0.10$
$\log \xi$	3	$2.00 \pm 0.04$	$1.69 \pm 0.03$	$1.73 \pm 0.06$
$v$	3	$-2200 \pm 100$	$0^f$	$0^f$
$N_{\text{H}}$	4	–	$22.00^f$	$21.29 \pm 0.08$
$\log \xi$	4	–	$1.78 \pm 0.03$	$1.39 \pm 0.05$
$v$	4	–	$-1730 \pm 50$	$-1910 \pm 140$
$N_{\text{OVII}}$		17.81	18.11	17.95
$N_{\text{OVIII}}$		18.14	18.20	17.97
$\chi^2/dof$		1.271 (8412.6 / 6620)	1.377 (16601.9/12053)	1.243 (14977.3 / 12051)

<sup>f</sup> -fixed.

well reproduced, the region across the 0.7 keV drop is poorly fitted since no Fe L-shell absorption is included. Adding FeI to account for the  $L_{2,3}$  edge clearly seen in the data ( $N_{\text{FeI}} = 10^{17.2} \text{cm}^{-2}$ ) produces a fit with  $\chi^2 = 17534.6/12051 \text{ dof}$ . See Table 2 (model 2) for fit parameters. The effects of warm absorption are now included by adding absorption by OVI-OVIII, FeXVII-XXIV and NeIX-X in two velocity components, one with an outflow velocity of  $\sim 2000 \text{ km s}^{-1}$  and the other at rest in the frame of the source as was observed by Sako et al. (2003). Also included is a broad Gaussian absorption trough at  $\sim 0.75 \text{ keV}$  to represent any Fe UTA. Allowing the columns of these species and FeI to be free parameters improves the fit ( $\chi^2 = 17579.4/12022$ ; see Fig. 7b). Table 2 (model 3) gives the fit parameters for this model. The OVIII column density of  $10^{18.4} \text{cm}^{-2}$  produces an edge at 0.871 keV with  $\tau \sim 0.24$ . The best-fitting column of FeI required is insufficient to account for the fine structure seen at 0.7 keV (see Fig. 6b) and the spectral index of the power-law is  $\sim 1.5$ , much lower than the  $\sim 2.0$  index found for the EPIC data (Fabian et al. 2002). The equivalent widths of the three emission lines are  $\sim 34 \text{ eV}$  for CVI Ly $\alpha$ ,  $\sim 38 \text{ eV}$  for NVII Ly $\alpha$  and  $\sim 220 \text{ eV}$  for OVIII Ly $\alpha$ .

Under the REL model of Sako et al. (2003) the 1.0–1.7 keV region consists of a power-law modified by narrow absorption features. Here we fit this region to a power-law producing a best-fitting spectral index of  $\Gamma = 0.93 \pm 0.04$ . Even with a column of FeI of  $10^{17.2} \text{cm}^{-2}$  the best-fitting spectral index is  $1.10 \pm 0.04$ . In order to match the continuum here with the softer power-law found at higher energies the continuum is required to break at around 2 keV from a hard power-law below the break to a softer one above. No mechanism is known that can create such a break.

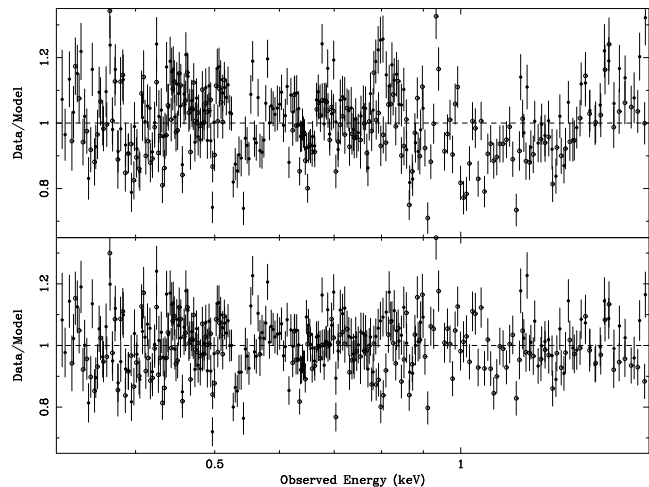


**Figure 7.** Ratio of data from RGS1 (filled circles) and RGS2 (open circles) to the best fitting REL models. Only data for orbit 301 is shown here. (a) Relativistically blurred emission lines and power-law (b) Relativistically blurred emission lines and power-law with warm absorption.

### 5.3 Combined DWA/REL model

Finally the DWA model was combined with the REL model and fitted to the data. It was found that the best fitting model obtained from the fit was strongly dependant on the starting position of the fit. If the REL model with zero line normalisation was added to the best fitting DWA model (model 2) then only very small emission lines were required. When the DWA model was added to the best

**Table 2.** Results of fits of the REL model to all three revolutions of RGS data. Equivalent widths of the emission lines ( $EW$ ) are given in eV, disc radii ( $R_{\text{in}}$  and  $R_{\text{out}}$ ) are given in units of  $r_g$ , inclination ( $i$ ) is given in degrees and column density ( $N_{\text{H}}$ ) is given in units of  $\log \text{cm}^{-2}$ .

model	1	2	3
$\Gamma$	$1.46 \pm 0.02$	$1.75 \pm 0.03$	$1.50 \pm 0.04$
$EW_{\text{CVI}}$	$35.2 \pm 12.7$	$27.6 \pm 5.2$	$34.1 \pm 10.0$
$EW_{\text{NVII}}$	$59.6 \pm 3.6$	$16.2 \pm 3.8$	$38.4 \pm 15.5$
$EW_{\text{OVIII}}$	$417.3 \pm 7$	$167.7 \pm 4.2$	$218.3 \pm 9.3$
$q$	$3.81 \pm 0.02$	$4.68 \pm 0.07$	$3.79 \pm 0.08$
$R_{\text{in}}$	$2.42 \pm 0.01$	$1.90 \pm 0.27$	$2.11 \pm 0.02$
$R_{\text{out}}$	$185 \pm 85$	$13.69 \pm 3.60$	$11.2 \pm 0.3$
$i$	$37.3 \pm 0.15$	$45.1 \pm 0.18$	$40.0 \pm 0.2$
$N_{\text{H}}(\text{FeI})$	–	$17.2^f$	$16.78 \pm 0.03$
$N_{\text{H}}(\text{OVII})$	–	–	$17.32 \pm 0.08$
$N_{\text{H}}(\text{OVIII})$	–	–	$18.39 \pm 0.03$
$\chi^2/dof$	1.449 (17457.8/12051)	1.455 (17534.6/12051)	1.310 (15749.4/12022)

<sup>f</sup> -fixed.

fitting REL model (model 1) then very little warm absorption was required. It would appear that two separate solutions exist; one with a large DWA and small REL and the other with small DWA and large REL.

#### 5.4 DWA/REL fitting summary

The REL model by itself is a poor fit and requires the addition of a DWA. Even then some parameters are unphysical. The simple DWA model, acting on a power-law continuum, probably requires structure in the soft X-ray continuum. The likely best-fitting model is a DWA acting on a continuum with some emission structures.

## 6 EMPIRICAL ABSORPTION MODEL

The principal difficulty in fitting the soft X-ray spectra of absorbed Seyfert 1 AGN is that the shape and level of the continuum is not known, partly because broad emission lines can mimic absorption edges. In this section we attempt to circumvent this problem using the known spectral variability of MCG–6-30-15.

The flux in the Fe  $K\alpha$  line at  $\sim 6.4$  keV is observed to vary little while the flux in the continuum is highly variable (Lee et al. 2000; Vaughan & Edelson 2001; Lee et al. 2002; Shih, Iwasawa, & Fabian 2002; Fabian et al. 2002). If a spectrum extracted from a period of low continuum flux is subtracted from a spectrum extracted from a period of higher flux, the resulting spectrum (the difference spectrum) can be adequately fit by just a power-law above  $\sim 2$  keV (Fabian et al. 2002). It would therefore appear that above  $\sim 2$  keV the emission consists of a rapidly variable power-law with constant Fe  $K\alpha$  emission. On this basis Fabian & Vaughan (2003) introduce a model for the emission consisting of a rapidly variable Power-Law Component (PLC) and an almost constant Reflection Dominated Component (RDC). Since the RDC changes little, subtracting a low flux spectrum from a high flux spectrum effectively removes it.

Data from revolution 303 were used to examine this variability for the RGS data since the flux level varied considerably during this period (see Vaughan et al. 2003 for light curves). Two pn spectra were extracted, one from the first 80 ks when the mean flux

level was high and one from the last 40 ks when the mean flux level was low. The low flux spectrum was subtracted from the high flux spectrum and the resulting difference spectrum was found to be adequately fitted by a power-law with  $\Gamma \sim 2.2$  in the range 3–10 keV. The ratio of data to best fitting power-law is shown in Fig. 8a. Assuming that the variability model applies to any reflection components below 3 keV, the underlying continuum in the pn difference spectrum is just a power-law and any deviations that are seen in Fig. 8a are due to absorption. These deviations from the high energy power-law therefore represent the absorption function of the source, including both intrinsic and Galactic absorption.

Next RGS spectra for the first 80 ks and last 40 ks of revolution 303 were extracted. The RGS spectra from the low flux period was subtracted from the RGS spectra from the high flux period for each instrument to leave the PLC modified by absorption. These RGS difference spectra were then divided by a power-law, with the spectral index and normalization fixed to the values derived from the pn difference spectrum, to produce the RGS absorption functions in Fig. 8b and c. The OI edge at  $\sim 0.54$  keV and the FeI/OVII edge at  $\sim 0.7$  keV can clearly be seen. This absorption function is compared to the best-fitting DWA absorption model from section 5.1 in Fig. 9a where the best-fitting DWA model is seen to be more absorbed than the absorption function inferred from the pn difference spectrum. This would result if the varying PLC is a broken power-law with a break at  $\sim 1-2$  keV and a softer spectrum below this break than that inferred from the pn difference spectrum in the 3–10 keV range. Fig. 9b compares the empirical absorption function obtained by assuming the PLC to be a broken power-law with slopes  $\Gamma_1 = 2.66$ ,  $\Gamma_2 = 2.29$  and break energy  $E_{\text{br}} = 1.75$  keV, with the best-fitting DWA model. Good agreement is found. Also if the best fitting DWA model is applied to the pn difference spectrum a broken power-law for the underlying continuum produces a good fit to the data. Fig. 10 shows the different model components present in the spectra.

We proceed by assuming that the absorption function for the soft X-ray spectrum is the pattern of deviations in the RGS difference spectrum from a broken power-law. This will be the case if the variable part of the spectrum is approximately a broken power-law continuum. Specifically this means that any additional emission features do not vary with the continuum, which would

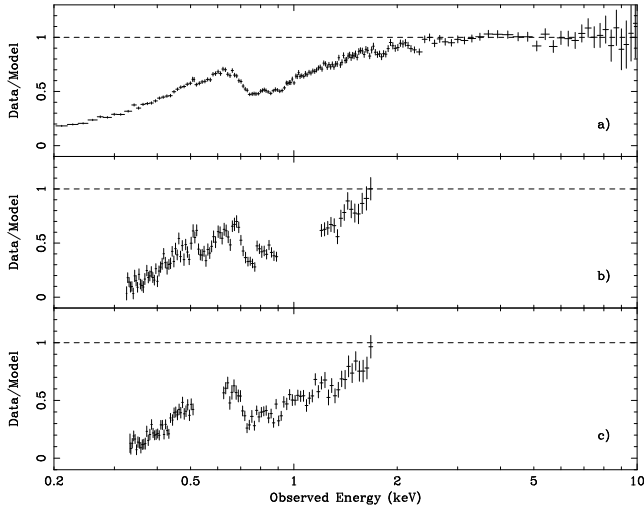


**Figure 8.** (a) Data/model ratio plot from fitting the pn difference spectrum to a power-law in the range 3–10 keV, excluding Galactic absorption. (b) Data/model ratio plot for the RGS1 difference spectrum compared to the model from (a). (c) Same as (b) except for the RGS2 difference spectrum. The gaps in the RGS data are due to nonfunctional chips in the detectors.

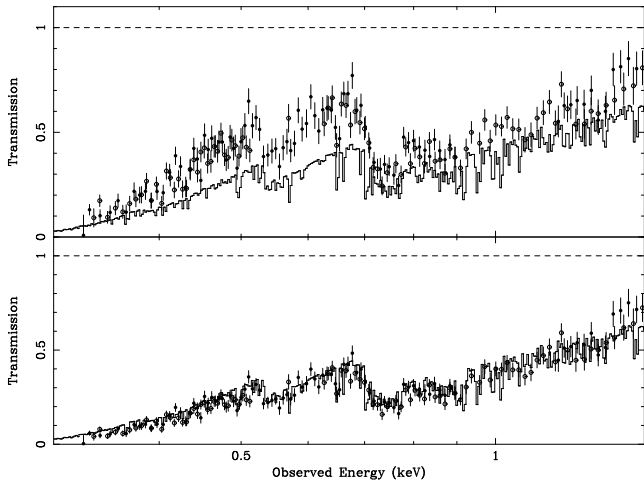


**Figure 9.** Empirical absorption function derived from RGS1 (filled circles) and RGS2 (open circles) compared to the best fitting DWA model absorption model (solid line). (a) Absorption function derived from the pn difference spectrum. (b) Absorption function derived from a broken power-law.

mean they contribute to the reflection dominated component of Fabian & Vaughan (2003). The assumption is supported by the fact that the RMS variability spectrum shows no sharp emission or absorption features below 1 keV (Fabian et al. 2002) and is well represented by the above model. The spectral indices and break energy of the broken power-law are assumed to be fixed while the normalization varies. Such a continuum is observed in many other Seyfert 1 X-ray spectra. The RGS difference spectra are divided by the broken power-law to form the RGS absorption function. Now that the absorption function has been derived for the soft X-ray band, its effects can be removed from the RGS data for the whole observation and the RDC in the soft-band can be examined. RGS data for all three revolutions were divided by the absorption function to correct for both Galactic and warm absorption. The spectra for each revolution were then fitted to a power-law and the ratio of data to best fitting model for each revolution combined to produce Fig. 11.

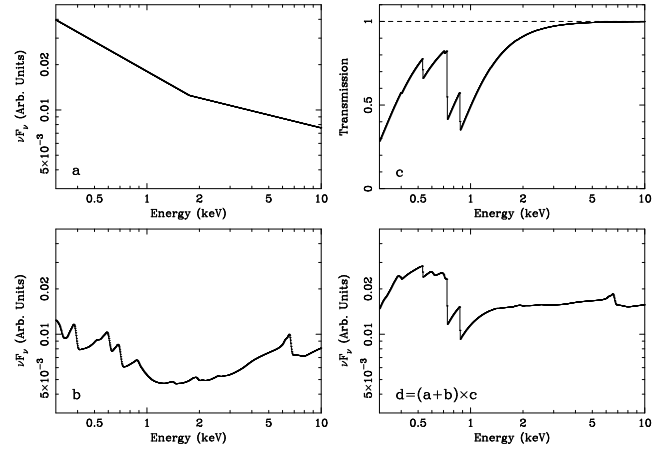


**Figure 10.** Model components present in spectra. (a) Power-Law Component (PLC). (b) Reflection Dominated Component (RDC) showing strong Fe K $\alpha$  emission and weaker soft X-ray emission lines. (c) Dusty Warm Absorber (DWA) showing strong OVII and OVIII edges. (d) Combination of all model components. N.B. This diagram is purely schematic and does not represent the actual model components.

The photon index of the best fitting power-law for the absorption corrected spectra was  $\sim 2.8$ , which is steeper than that derived for the high energy spectral index of the PLC of  $\sim 2.3$ , re-enforcing the idea that there may be a soft excess below 2 keV, similar to the variable two component power-law in Ton S180 (Vaughan et al. 2002). The residuals also show an excess of emission below 0.4 keV and a trough at  $\sim 1$  keV. Any features around the OVII (0.5740 keV) or OVIII (0.6536 keV) emission lines are constrained to be less than  $\sim 20$  per cent of the continuum. Provided the PLC continuum is a power-law in the RGS passband, the shape of the residuals in Fig. 11 are independent of the spectral index and normalization assumed for that power-law. Note the resemblance to the residuals found earlier (Fig. 5a).

The whole emission complex between 0.45 and 0.9 keV was earlier modelled as a broad Gaussian (section 5.1). We now fit it in the absorption corrected spectra with a power-law and emission lines centred on the OVII  $1s^2 - 1s2p$  and OVIII Ly $\alpha$  line energies. Fits with both intermediate width Gaussian and relativistically-blurred lines produce upper limits on the equivalent width of OVII and OVIII emission of  $\sim 30$  eV. The whole complex could be due to OVII, OVIII, FeL and other emission expected in the reflection spectrum (Ballantyne et al. 2002) together with further absorption structure. Detailed modelling of this emission will be carried out in later work.

## 7 DISCUSSION

The high signal-to-noise of our 320 ks observation has allowed the unambiguous detection of FeL L-shell absorption through the fine structure at the L<sub>2,3</sub> edge. This has been observed before in the ISM (Paerels et al. 2001) and in Cygnus X-1 (Schulz et al. 2002). It combines with the resonance and edge absorption from OVII and OVIII to explain the drop in flux at 0.7 keV (Lee et al. 2001) and remove the  $\sim 16,000$  km s<sup>-1</sup> discrepancy in position between the observed drop and that expected from the OVII K-shell edge reported in Branduardi-Raymont et al. (2001).

In comparing the DWA and REL models to the data, both produce similar values of  $\chi^2$ , although all models are formally un-

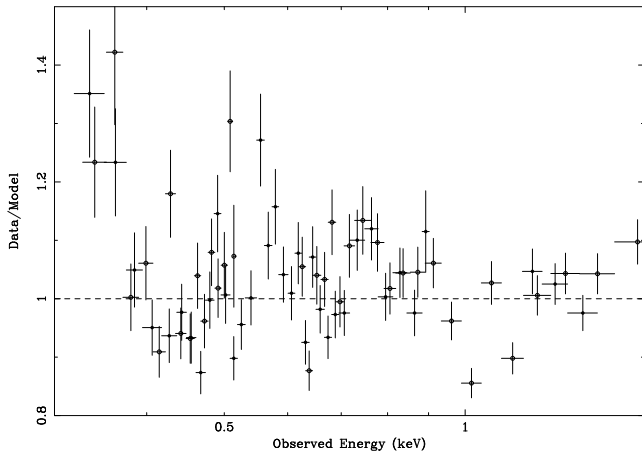


**Figure 11.** Combined ratio of the absorption corrected data from RGS1 (filled circles) and RGS2 (open circles) to the best-fitting power-law for all three orbits.

acceptable. However the normalizations of the three broad emission lines in the REL model are free parameters, so the level of the continuum in each section of the spectra can be easily fit. The equivalent widths of these lines are also much larger than has been obtained with self-consistent models of ionized disc reflection (Ballantyne et al. 2002). As has been noted in Section 5, the best-fitting REL model requires insufficient FeI to fit properly the fine structure at 0.7 keV and produces an unrealistically flat spectral index for the underlying power-law. The DWA model in contrast uses only a broken power-law for the underlying continuum. Addition of a reflection component, with emission features around the 10–20 per cent level (Fig. 11), may well explain some of the remaining residuals (see for example the model in Fabian & Vaughan 2003). The DWA model also assumes Solar abundances and a turbulent velocity of  $100 \text{ km s}^{-1}$ . Relaxing these two assumptions should improve the fit further. These improvements will be explored in a later paper.

In Section 6 the pn and RGS difference spectra are used to determine the presence of additional emission components. This method reveals a steep increase in flux below 0.4 keV and a trough at 1 keV. This suggests that an extra emission component is present below 0.4 keV which, combined with increased low ionization parameter warm absorption, could explain the low energy residuals from the DWA model. This extra emission component may be the high energy tail of the quasi-blackbody emission emitted from the accretion disc. These methods assume the absorption present is non-varying, whereas an anti-correlation of the optical depth of an absorption feature with ionizing flux would produce a drop in the absorption corrected spectra where that absorption was. Such variability was observed by Otani et al. (1996) for absorption around 1 keV. The residuals in the DWA fit at 1 keV may be due to a warm absorber zone with this sort of variability which would explain the trough seen at  $\sim 1$  keV in the absorption corrected spectra. The fact that no large peak in the absorption spectra is observed in the 0.6–0.7 keV region suggests that any OVIII emission, which does not vary exactly with the continuum, is at a level not greater than  $\sim 10$ –20 per cent of the continuum. This is much smaller than in the basic REL model.

In summary, we have found that detailed absorption modelling of the average RGS spectra agrees with an analysis based on variability. Both indicate the dominant presence of dusty warm absorber. Residuals from the modelling show that the underlying con-

tinuum has some complex emission structures in the 0.4–0.9 keV band of amplitude consistent with theoretical predictions for an ionized reflector.

## ACKNOWLEDGEMENTS

Based on observations obtained with *XMM-Newton*, an ESA science mission with instruments and contributions directly funded by ESA Member States and the USA (NASA). AKT acknowledges support from PPARC. ACF thanks the Royal Society for support. JCL thanks the Chandra fellowship for support. This was provided by NASA through the Chandra Postdoctoral Fellowship Award number PF2-30023 issued by the Chandra X-ray Observatory Center, which is operated by SAO for and on behalf of NASA under contract NAS8-39073. We thank Gary Ferland for help with CLOUDY Jeff Kortright for useful information on the FeI L edge profile and an anonymous referee for helpful comments.

## REFERENCES

- Arnaud K., 1996, in *Astronomical Society of the Pacific conference series*, Vol. 101, Jacoby G. H., Barnes J., ed, *Astronomical Data Analysis Software and Systems*, p. 17
- Ballantyne D. R., Ross R. R., Fabian A. C., 2002, *MNRAS*, 336, 867
- Behar E., Sako M., Kahn S. M., 2001, *ApJ*, 563, 497
- Branduardi-Raymont G., Sako M., Kahn S. M., Brinkman A. C., Kaastra J. S., Page M. J., 2001, *A&A*, 365, L140
- Elvis M., Wilkes B. J., Lockman F. J., 1989, *ApJ*, 97, 777
- Fabian A. C., Vaughan S., 2003, *MNRAS*, in press (astro-ph/0301588)
- Fabian A. C. et al., 2002, *MNRAS*, 335, L1
- Ferland G. J., Korista K. T., Verner D. A., Ferguson J. W., Kingdon J. B., Verner E. M., 1998, *PASP*, 110, 761
- George I. M., Turner T. J., Netzer H., Nandra K., Mushotzky R. F., Yaqoob T., 1998, *ApJS*, 114, 73
- Kortright J. B., Kim S.-K., 2000, *Phys. Rev. B*, 62, 12216
- Laor A., 1991, *ApJ*, 376, 90
- Lee J. C., Fabian A. C., Reynolds C. S., Brandt W. N., Iwasawa K., 2000, *MNRAS*, 318, 857
- Lee J. C., Iwasawa K., Houck J. C., Fabian A. C., Marshall H. L., Canizares C. R., 2002, *ApJ*, 570, L47
- Lee J. C., Ogle P. M., Canizares C. R., Marshall H. L., Schulz N. S., Morales R., Fabian A. C., Iwasawa K., 2001, *ApJ*, 554, L13
- Mewe R., 1977, *A&A*, 59, 275
- Nayakshin S., Kazanas D., Kallman T. R., 2000, *ApJ*, 537, 833
- Nicastro F., Fiore F., Matt G., 1999, *ApJ*, 517, 108
- Otani C. et al., 1996, *PASJ*, 48, 211
- Paerels F. et al., 2001, *ApJ*, 546, 338
- Różańska A., Dumont A.-M., Czerny B., Collin S., 2002, *MNRAS*, 332, 799
- Reynolds C. S., 1997, *MNRAS*, 286, 513
- Ross R. R., Fabian A. C., 1993, *MNRAS*, 261, 74
- Sako M. et al., 2003, *ApJ*, accepted (astro-ph/0112436)
- Schulz N. S., Cui W., Canizares C. R., Marshall H. L., Lee J. C., Miller J. M., Lewin W. H. G., 2002, *ApJ*, 565, 1141
- Shih D. C., Iwasawa K., Fabian A. C., 2002, *MNRAS*, 333, 687
- Vaughan S., Boller T., Fabian A. C., Ballantyne D. R., Brandt W. N., Trümper J., 2002, *MNRAS*, 337, 247



- Vaughan S., Edelson R., 2001, ApJ, 548, 694  
Vaughan S., Fabian A. C., Nandra K., 2003, MNRAS, 339, 1237  
Verner D. A., Verner E. M., Ferland G. J., 1996, Atomic Data and  
Nuclear Data Tables, 64, 1  
Verner D. A., Yakovlev D. G., 1995, A&AS, 109, 125